university of groningen

University Medical Center Groningen

University of Groningen

A novel method for determining the Femoral-Tibial Angle of Knee Osteoarthritis on X-ray radiographs

Wahyuningrum, Rima Tri; Purnama, I Ketut Eddy; Verkerke, Gijsbertus Jacob; van Ooijen, Peter M A; Purnomo, Mauridhi Hery

IMPORTANT NOTE: You are advised to consult the publisher's version (publisher's PDF) if you wish to cite from it. Please check the document version below.

Document Version
Publisher's PDF, also known as Version of record

Link to publication in University of Groningen/UMCG research database

Research article

A novel method for determining the Femoral-Tibial Angle of Knee Osteoarthritis on X-ray radiographs: data from the Osteoarthritis Initiative

Rima Tri Wahyuningrum [a,c], I Ketut Eddy Purnama [a,b], Gijsbertus Jacob Verkerke [d,f], Peter M.A. van Ooijen [e], Mauridhi Hery Purnomo [a,b,g,*]

[a] Department of Electrical Engineering, Institut Teknologi Sepuluh Nopember, Surabaya, Indonesia
[b] Department of Computer Engineering, Institut Teknologi Sepuluh Nopember, Surabaya, Indonesia
[c] Department of Informatics, Universitas Trunojoyo Madura, Bangkalan, Indonesia
[d] Department of Rehabilitation Medicine, University of Groningen, University Medical Center Groningen, the Netherlands
[e] Department of Radiation Oncology, University of Groningen, University Medical Center Groningen, the Netherlands
[f] Department of Biomechanical Engineering, University of Twente, the Netherlands
[g] The Science and Technology Center of Artificial Intelligence for Healthcare and Society (PUI AI HeS), Indonesia

ARTICLE INFO

ABSTRACT

Femoral-tibial alignment is a prominent risk factor for Knee Osteoarthritis (KOA) incidence and progression. One way of assessing alignment is by determining the Femoral-Tibial Angle (FTA). Several studies have investigated FTA determination; however, methods of assessment of FTA still present challenges. This paper introduces a new method for semi-automatic measurement of FTA as part of KOA research. Our novel approach combines pre-processing of X-ray images and the use of Active Shape Model (ASM) as the femoral and tibial segmentation method, followed by a thinning process. The result of the thinning process is used to predict FTA automatically by measuring the angle between the intersection of the two vectors of branching points on the femoral and tibial areas. The proposed method is trained on 10 x-ray images and tested on 50 different x-ray images of the Osteoarthritis Initiative (OAI) dataset. The outcomes of this approach were compared with manually obtained FTA measurements from the OAI dataset as the ground truth. Based on experiments, the difference in measurement results between the FTA of the OAI and the FTA obtained using our method is quite small, i.e., below 0.81° for the right FTA and below 0.77° for the left FTA with minimal average errors. This result indicates that this method is clinically suitable for semi-automatic measurement of the FTA.

1. Introduction

Osteoarthritis (OA) is a disease that affects the joints and surrounding structures. OA is a chronic disease; however, appropriate therapy and proper medical treatment can reduce the pain associated with this condition. According to WHO data (2017), the prevalence of this disease is increasing yearly in developed countries. Global estimates indicate that 18.0% of women and 9.6% of men aged over 60 years have osteoarthritis [1]. The most common osteoarthritis is Knee Osteoarthritis (KOA). The pain that arises from KOA reduces the quality of life and restricts daily activities. Furthermore, KOA can cause depression and anxiety, as well as a considerable economic burden. For example, in the United States (US), the healthcare expense associated with this condition is estimated at US$ 186 billion annually [2].

In general, medical experts and researchers are using the information from imaging obtained with multiple modalities for assessment of KOA. Although high-resolution MRI has quickly advanced as a popular method, it has a low availability and high cost. Hence, radiography is regarded as the gold standard to appraise disease severity of KOA, since it is non- or minimally invasive, inexpensive, appropriate, and can be performed quickly [2, 3, 4].

A fundamental issue in KOA is verifying the severity of the disease. The Kellgren-Lawrence [5] classification of the severity of KOA is based on the following five parameters: the presence of osteophytes on the joint margins; the presence of periarticular ossicles, mainly in relation to distal and proximal interphalangeal joints; narrowing of joint cartilage associated with subchondral bone sclerosis; small pseudocyst areas with sclerotic walls, usually located in the subchondral bone; and altered

---

* Corresponding author.
  E-mail address: hery@ee.its.ac.id (M.H. Purnomo).

shape of the bone ends, especially in the head of femur. Subsequently, the severity of KOA based on Kellgren-Lawrence is categorized into five stages. Stage 0 represents normal and healthy knees, stage 1 represents doubtful OA, stage 2 is indicative of mild OA, stage 3 represents moderate OA, and stage 4 is indicative of severe OA. Numerous experiments have demonstrated successful methods to establish the severity of KOA [4, 5, 6, 7, 8]. However, there is no accurate method for measuring the severity of KOA in general clinical practice. In addition, current research shows that Trabecular Bone Texture (TBT) parameters measured on computed radiography may be useful to identify patients at risk for OA, target therapy in OA, detect the development of knee OA, and predict the onset of tibiofemoral OA (knee) [9, 10, 11]. These parameters show promising results in identifying at risk patients for future clinical trials.

Semi-automatic techniques for objective measurement using continuous variables of joint space or angle applying computer-aided systems have been previously reported. However, intra-observer and inter-observer variability remain a problem since initial operations such as recognizing points or drawing lines are performed manually [12, 13, 14, 15, 16, 17, 18]. A computer-assisted method to determine Femoral-Tibial Angle (FTA) was proposed earlier in the literature [12]. Takahashi et al. [12] used manually drawn lines from four selected points at each of the two levels of the cortical margins to assess the femoral axis. Similarly, four points must be selected to draw the lines required to determine the tibial axis. Based on these manual inputs, the FTA can be calculated. Oka et al. [13] proposed a femoral axis and a tibial axis determined from a straight regression line. This line was drawn from the midline between the medial and lateral outlines of the femur from the top of the image to the inflection points. Similarly, for the tibial axis, the line was drawn from the midline of the tibia from the bottom of the image to the inflection points. Thereafter, the FTA is calculated as the lateral angle between two lines.

Furthermore, Wong et al. [14] presented the determination of the anatomic FTA by placing three lines manually namely the midline, the femoral line, and the tibial line. The midline is a line centered at the tibial tips. While the other two lines, each placed 10 uation determined by Krae

with the endpoints on the outer cortical skin that is aligned parallel to the femoral condyles and tibial plateau. Then the FTA measurement is done by converting the anatomical angle into a mechanical angle using the equation determined by Kraus. Hereafter, McDaniel et al. [15] conducted a comparison of five approaches for measuring the FTA. The difference between the five approaches is the placement of the points that become the reference in calculating the FTA. Among the five approaches (method A - E), McDaniel et al. [15] only recommends two methods, namely methods B and C. Both methods use only one reference point. Specifically, in method B, the reference point is placed at the center of the base of the tibial spines; meanwhile, in method C, the reference point is placed at the midpoint of the tibia, which is determined by a line connecting the lateral and medial margins of the tibial plateau. Furthermore, the FTA is determined from the femur and tibia centerline intersections based on the knee center point.

Meanwhile, Sheehy et al. [16] used the Femoral Shaft – Tibial Shaft (FS-TS) angle from knee radiographs to estimate Hip Knee Ankle (HKA) angle. The FS-TS angle is the angle between the anatomic axis of the femur and tibia. In addition to measuring FTA, Iranpour-Boroujeni et al. [17] have a different way. FTA does not depend on the crossing point because it is projected as an angle made from the femoral and tibial axis. The femoral axis is upright to the basic line of the femoral condyles and is centered inside the outer borders of the medial and lateral femoral epicondyles. In this case, the axis is the line connecting the midpoint of the labelled area. Meanwhile, this study also defines the tibial axis as a line obtained from two points on the tibial bone. Namely by positioning the first point at 10 mm and the second point at 100 mm below the projected tibia plateau. Meanwhile, Goulston et al. [18] used anatomical axis knee alignment measurements by comparing the one-point and two-point methods using the Knee Joint Centre (KJC). After establishing the center line on the femur and tibia at 10 cm from the center of the knee joint, an FTA measurement is performed based on the intersection of the two midlines.

All the FTA determination methods described are semi-automatic (combination of manual and automatic steps). The manual step
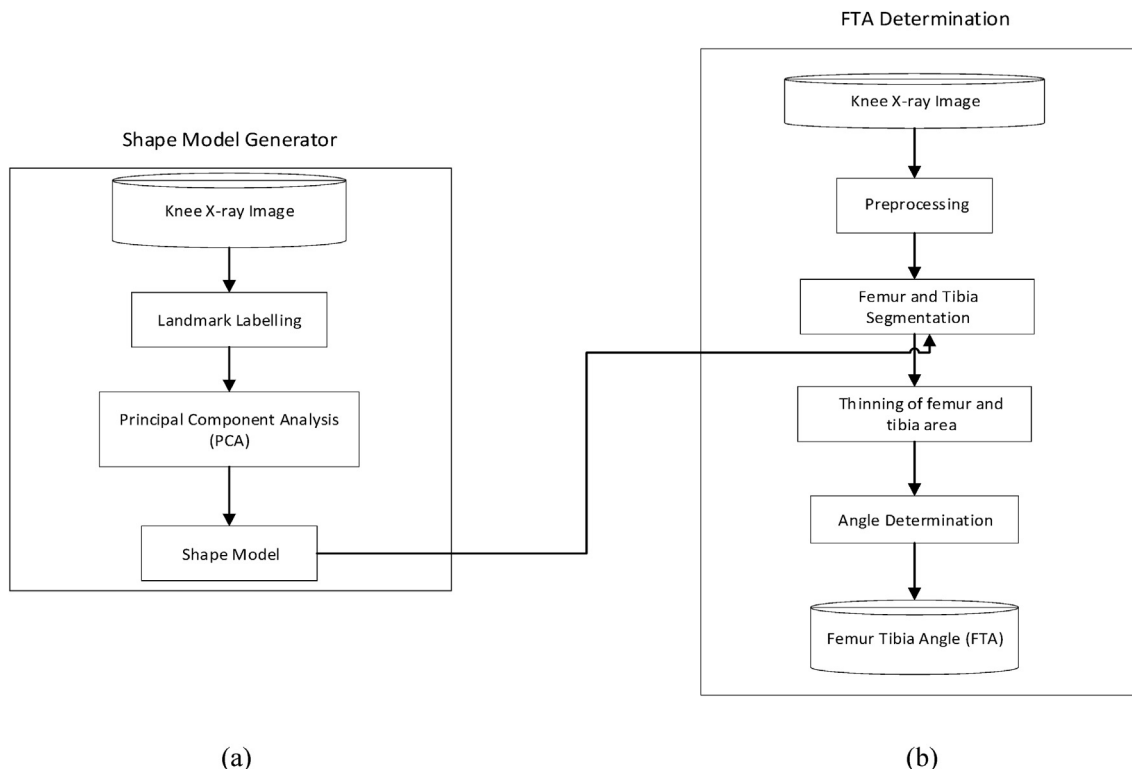

Figure 1. The proposed method: (a) Shape model generator, (b) FTA determination.

consists in the determination of one, two, or four points and/or one or two lines on the femur and tibia. Subsequently, FTA calculations are performed automatically. In addition, all FTA measurement methods that have been carried [12, 13, 14, 15, 16, 17, 18] did not involve patients with femoral tibial bowing. The purpose of this study was to present a new method for semi-automatic measurement of the FTA, since malalignment based on FTA is a risk factor for KOA [19]. In addition, orthopedic surgeons can also use the method for determining FTA proposed in this study to check postoperative alignment regularly.

We propose an image processing method to determine FTA with only minimal user interaction. Different from previous methods, the only manual interaction required involves a single click to position an average shape on each image. This method is carried out in several stages. First, pre-processing is performed with image dimension normalization and image enhancement using the contrast stretching method. Second, segmentation of the femur-tibia is performed using Active Shape Model (ASM). Third, thinning from the femur-tibia segmentation is performed using Hit Miss Transformation (HMT) using an erosion and dilation method. Finally, the FTA is determined automatically with the method we have developed.

2. Materials and methods

In this study, all the experimental datasets were acquired from the OAI dataset (http://www.oai.ucsf.edu/), which includes MRI and radiography results. We randomly selected 60 knee radiographic images from this dataset, which have almost the same brightness and distribution of the histogram. All images obtained were normalized to the standard dimension of 3484×4262. Subsequently, these images were split into two subsets, 10 training images and 50 testing images, and each image was separated into right and left knee, respectively. The training images were used for pattern learning to obtain a shape model of the bones and angle measurement, while the testing images were used to assess the performance of our method.

The proposed method included pre-processing, segmentation, thinning, and measurement of the FTA automatically. Figure 1(a) illustrates the procedure used to create a shape model of the femoral and tibial area, which is required in the segmentation step in the proposed FTA determination method. Figure 1 (b) explains the process of obtaining the FTA. A more detailed explanation of the proposed method is provided in the subsequent sections of this paper.

2.1. Preprocessing

The purpose of image normalization is to equate the dimensions of all images while increasing the processing speed. The normalization is performed by removing boundary pixels to obtain the desired size. In this study, the standard dimension used is 4262×3484. The next step of the process is to perform image enhancement. The quality of the image is an essential element, since it may affect the performance of the overall algorithm [20, 21]. The images from the OAI database have been collected from various radiographic centers, resulting in large differences in intensity due to the use of x-rays and different recording equipment. In this study, there were 43 images among the 60 images used in this study that present low brightness and contrast. Therefore, we applied contrast stretching automatically to improve image quality and to clarify the shape of the femur-tibia. Figure 2 illustrates an example of a preprocessing image.

Figure 2 (a) is an example of one image used in this study. Meanwhile Figure 2 (b) is the result of image enhancement of Figure 2 (a) using the contrast stretching method. Figure 2 (b) looks brighter and clearer than Figure 2 (a). Therefore, the use of this method can improve image clarity for the next step in the research process.

2.2. Segmentation

The segmentation step aims to determine the boundary of the femoral and tibial areas. Segmentation is reported to be one of the most crucial steps in image processing [22, 23, 24]. Segmenting structure in the X-ray image is a difficult task. Currently, the segmentation method that is constrained by predefined shape is preferable. Therefore, in our work, we chose to use the ASM.

2.2.1. Segmentation using ASM

This method was first proposed by Cootes [25] and is one of the notable, deformable model-based segmentation methods. This method is attracting widespread interest for numerous segmentation assignments in medical images [22, 23, 26, 27]. The segmentation step using ASM consists of a substep to create the shape of the model as shown in Figure 1 (a).

In the ASM, a set of landmarks, which outline the object form, was used to define an object [26, 27, 28]. Each landmark is manually placed to represent the area of interest in each training image. Meanwhile, each
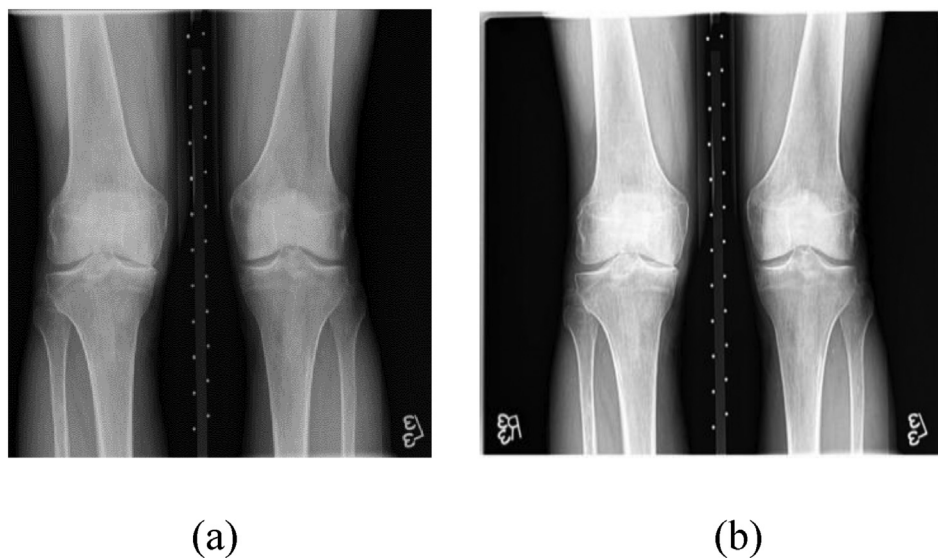

(a)   (b)

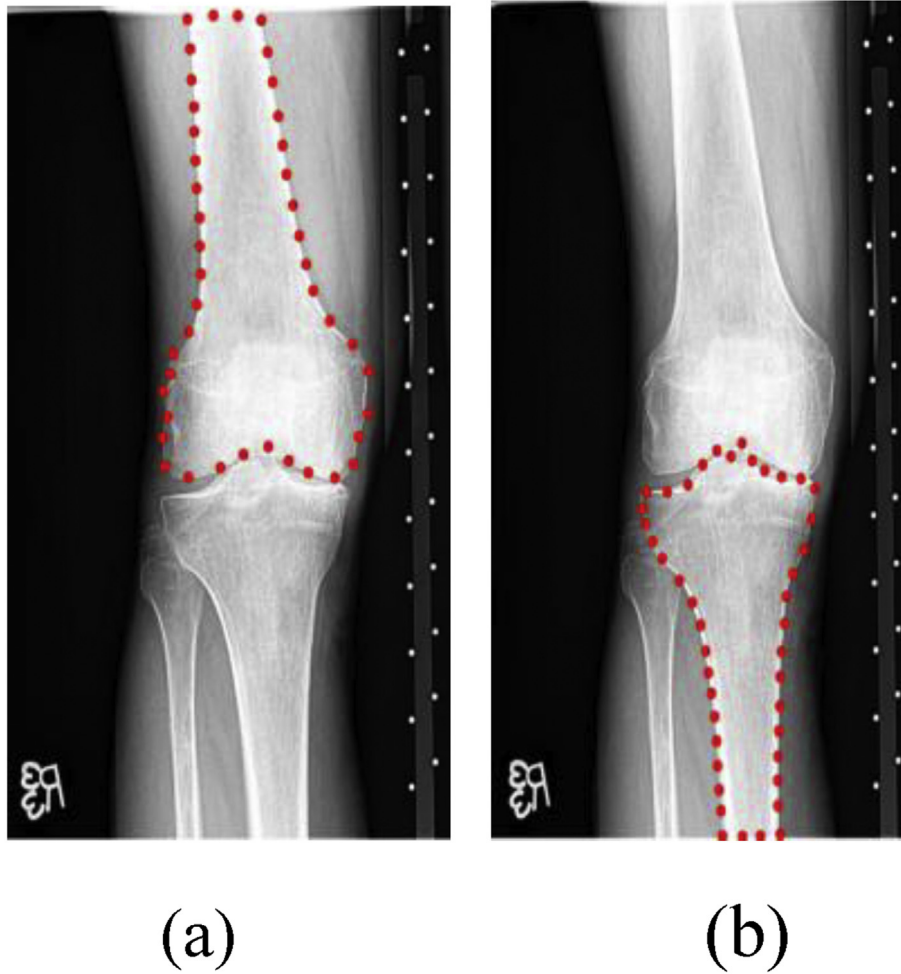**Figure 2.** A sample image (a) before, (b) after contrast stretching.

Figure 3. Forty-three landmarks used to form (a) right femoral shape (b) right tibial shape.

training image consists of coinciding landmarks. In this study, we used 43 landmarks to specify the femoral and tibial shapes. A set of landmarks is indicated as vector *A* as shown in Eq. (1). Each shape of training image (*A*) consists of landmarks where each coordinate point (*x, y*) with the order of points 1 to *n* and *A* is presented in vector form. *T* superscript in Eq. (1) shows the form of matrix transposition. Figure 3 shows an example of 43 landmarks used for training images to segment the right femoral and tibial shape.

$$A = (x_1, \ldots, x_n, y_1, \ldots, y_n)^T \tag{1}$$

Furthermore, scaling, rotating, and translating to minimize the sum of squared error between the landmark lengths were some methods used for alignment of vector *A*. Accordingly, the mean shape for the alignment of training shape ($\overline{A}$) and covariance of the matrix (*S*) was computed as follows:

$$\overline{A} = \frac{1}{s} \sum_{i=1}^{s} x_i \tag{2}$$

$$S = \frac{1}{s-1} \sum_{i=1}^{s} (x_i - \overline{x})(x_i - \overline{x})^T \tag{3}$$

where $\overline{A}$ is the average of *A* as shown in Eq. (2). $\overline{A}$ is also known as zero mean. *s* is the number of training images with sequence *i* starting from 1 to *s*. Meanwhile, x_i is the intensity value of pixels in the *i* training image. in Eq. (3) shows the average of x_i; meanwhile, *S* is a covariance matrix.

In this research, Principal Component Analysis (PCA) was used to determine the major axis of variation for the femoral and tibial bone correspondence landmarks in the 10 training images. This procedure is applied by using eigenvalue decomposition of the covariance matrix. A matrix *P*, where $P = (p_1|p_2|\ldots|p_t)$ is a matrix of new features obtained from the multiplication of eigenvectors corresponding to eigenvalues (λ_i), with a zeromean matrix ($\overline{A}$). While the eigenvectors and eigenvalues are obtained from the covariance matrix (*S*) in Eq. (3) uses Singular Value Decomposition (SVD) function in Matlab 2018b. *t* is the number of eigenvalues to retain to ensure that their sum is sufficient to explain the variance in the training shapes. Van Ginneken [26] recommended that the variance ranges should be defined from 90% to 99.5% of the sum of eigenvalues. To adhere to this recommendation, we used 98% of the sum of eigenvalues. Moreover, Eq. (4) was used for the approximation of the femoral and tibial forms in the training images:

$$A \approx \overline{A} + Pb \tag{4}$$

where *b* is a *t*-dimensional vector specified by

$$b = P^T(x - \overline{x}) \tag{5}$$

The values of *b* are set to be within the range of $\pm 3\sqrt{\lambda_i}$ to restrict newly generated shapes to be in the allowable shape domain.

Furthermore, the shape model was merged with the femoral and tibial images. The shape model was placed near the center location of the femoral and tibial area using a single-click manual interaction. The searching process was initialized from coarse searching to fine
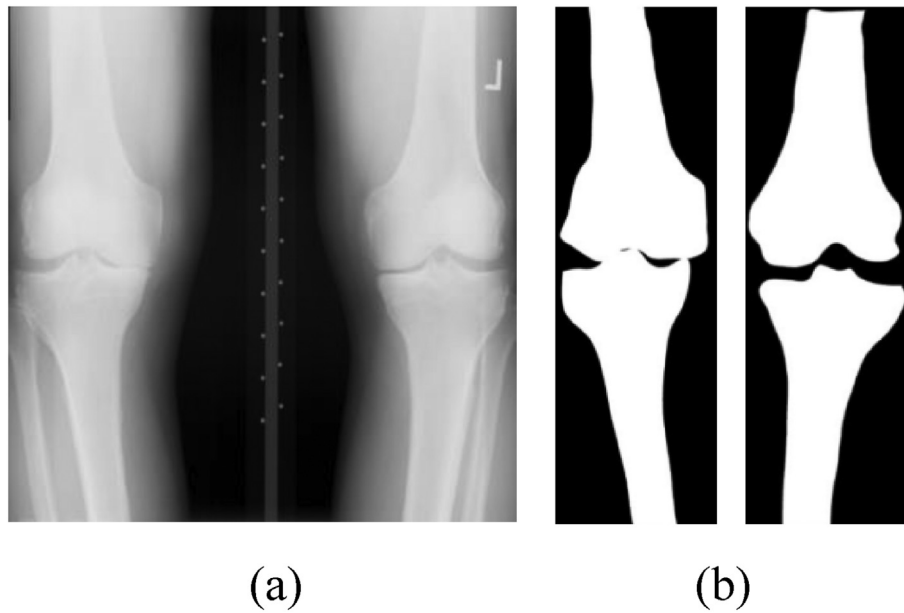
Figure 4. Image of the ASM process: (a) original image, (b) the binary segmentation result.

adjustment of each corresponding landmark to fit the shape of the femoral and tibial area in the knee X-ray image. Initialization was usually done using the mean shape with translation, rotation, and scale parameters close to their correct values. At each iteration, we consider points on and to either side of the contour along the normal direction. Subsequently, the landmark position is updated as the point with minimum Mahalanobis distance. After having processed all landmarks, the closest plausible shape was obtained by projecting the updated landmarks onto the eigenspace. The search process was halted once the set number of iterations was achieved. The obtained shape was then converted into a binary image to illustrate the shape of the femoral and tibial area as the visible object, while the remaining portion of the image is set as the background. Figure 4 (b) is an example of the results of the segmentation of the femur and tibia that are different from the previous image. In this figure, the femur and tibia are well segmented using the ASM.

2.2.2. Manual segmentation

Manual segmentation in this study is used as ground truth, which is a reference to compare with the computational method developed (ASM). The ground truth was obtained by complete manual delineation of the object boundaries by a human observer. The following are the steps in establishing ground truth: first, reading x-ray images of the knee to be segmented; second, changing the image to grayscale; third, resizing the image to 3484×4262 (the same size as ASM segmentation); fourth, displaying the x-ray image of the knee; fifth, manually drawing the edge of the femur-tibia with the help of the cursor; sixth, displays the image after being segmented; and, finally, saving the image.

2.2.3. Validation of the segmentation

To measure the accuracy of this segmentation method, this research uses Hausdorff Distance (HD) [29, 30]. The directed HD ($\widehat{H}$) between two point sets E and F is the maximum of distances between each point $x \, \varepsilon \, E$, and its nearest neighbor $y \, \varepsilon \, F$. That is

$$\widehat{H}(E, F) = \max_{x \in E}\left\{\min_{y \in F}\left\{\|x, y\|\right\}\right\} \qquad (6)$$

where $\|., .\|$ is any norm. Note that $\widehat{H}(E,F) \neq \widehat{H}(F,E)$ and thus the directed HD is not symmetric. H is the maximum of the directed HD in both directions, and, therefore, it is symmetric. H is given by Eq. (7):

$$H(E, F) = \max\left\{\widehat{H}(E, F), \widehat{H}(F, E)\right\} \qquad (7)$$

E is the point that represents ASM segmentation while F is the point that represents manual segmentation. To obtain these points, the algorithm used is the following:

D: ASM segmentation image or manual with size (b,c)
Temporary: zeros matrix of the same size as D
    for each pixel on D
    do matching with the edge operator
      if D (b,c) is not the same as the element on the operator
        D (b,c) is the edge
        Temporary ← D (b,c)
      else
        D (b,c) is not an edge

In this study, we proposed an edge operator with a scheme as shown in Figure 5. The definition of edge operator elements in the algorithm above is all pixel entries in Figure 5 other than pixel elements (b, c). The next step is measuring HD from the points surrounding the femur-tibia, which have been obtained both from the results of manual and ASM segmentation. HD measurements are calculated based on Eqs. (6) and (7). From these measurements, the results are in the form of pixels. Previously, raw data information (DICOM from OAI) was obtained by raw data interpolation, in which pixel resolution was 0.37 mm × 0.37

b-1,c-10	b-1,c	b-1,c+10
b,c-10	b,c	b,c+10
b+1,c-10	b+1,c	b+1,c+10

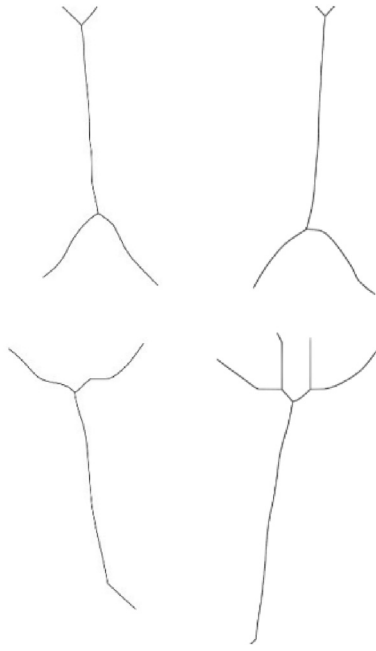**Figure 5.** The proposed edge operator elements.

Figure 6. An example of thinning result image using morphology operations.

mm (2 Dimensions = (x, y)). Therefore, the HD measurement results in the form of pixels are converted to units of mm.

Additionally, this research also used the Dice Similarity Coefficient (DSC). The DSC is a spatial overlap index and validation of matrix reproducibility. The DSC values range from 0 (indicating no spatial overlap between two sets of binary segmentation results) to 1 (indicating complete overlap) [31, 32, 33]. In this case, the DSC measures the spatial overlap between the two segments, the target areas A and B, where A is the result of manual segmentation (ground truth), B is the result of segmentation of the ASM method and $\cap$ is the intersection so that the DSC is defined as Eq. (8).

$$DSC = 2(A \cap B)/(A + B) \tag{8}$$

2.3. Thinning of the femoral and tibial area

Thinning or skeletonization is considered a pre-processing technique, which is one of the most crucial steps [34, 35]. Thinning is a process that peels pixels of a binary image as much as possible while preserving the connectivity of the original image. Moreover, this process also extracts image contours until it reaches the most medial one-pixel width. The purpose of thinning is to reduce unnecessary, or redundant, parts so that only the essential information is generated.

In the thinning procedures, we use a mathematical morphology operations. This operation is performed by utilizing the hit-and-miss operators, usually also called erode and dilate. The basic operations involved in HMT are complement, intersection, erosion, and dilation [34, 35]. The thinning of a set (C) by structure element (D), $\otimes$ denotes the convolution, so that $C \otimes D$ can be defined regarding HMT as shown in Eq. (9).

$$C \otimes D = C - (C \odot D) = C \cap (C \odot D)^c \tag{9}$$

where $C \otimes D$ is also designated as erosion, $(C \odot D)$ is designated as dilation, and $\cap$ is designated as an intersection; meanwhile, $(C \odot D)^c$ is the complement of $(C \odot D)$. A more useful expression for thinning C symmetrically is based on a Structuring Elements (SE) sequence of Eq. (10).

$$\{D\} = \{D^1, D^2, D^3, ..., D^n\} \tag{10}$$

where D^i is a rotated version of D^{i-1}. Meanwhile, $D^1, D^2, ..., D^n$ is a sequence of SE as a result of the rotation version of D^{i-1}. The SE commonly used are diamonds, squares, and hexagons. In this study, we used diamonds. We apply this concept to define thinning by a sequence of SE as follows:

$$C \otimes \{D\} = \left((..(C \otimes D^1) \otimes D^2)..) \otimes D^n \right) \tag{11}$$

The process involves thinning C once with D^1, then thinning the result once again with D^2, and repeating this process until C is thinned with once D^n. The entire process is repeated until no further changes occur. Each thinning pass is performed using Eq. (9). One example of the results of thinning is shown in Figure 6. The figure shows a successfully obtained midline of the femur and tibia. This image is needed for the next step, which is determining the FTA.

2.4. Automatic FTA determination

To perform FTA measurements automatically, we proposed a new method consisting of several steps:

1. The input image from the results of thinning. Make a color change for pixels (i) that is less visible (has a low-intensity value or i > 0) to 255 (white), in order to be easily distinguished.
2. Look for all pixels with an intensity value = 255, then save the row and column (coordinates) of the pixel. Searching for pixel intensity values is performed from the left row to the right row, then from the top column to the bottom column.
3. Sort pixel coordinates (which have intensity values 255) from small to large. The purpose of sorting coordinates is to make it easier to search branching points.
4. Record the points that will become candidate branches with conditions if there is the same value in each row. Then the column coordinates of the same row are also recorded. The following is the procedure:
   a. Look for white pixels with a greater quantity than 1 in each row.
   b. Next, subtract the last white pixel coordinate with the first white pixel coordinate to find the difference.
   c. If the difference is less than seven, it is not a branch; however, what is formed is a straight line from the results of femoral and tibial bone thinning, as shown in the red circle in Figure 7.
5. Next, the pixels or lines formed (as shown in Figure 7) are used to determine the starting point and end-point of branching, both in the femur and tibia. In this case, u_1 is the starting point of branching in the femur; u_2 is the end-point of branching in the femur; v_1 is the starting point of branching in the tibia, and v_2 is the end-point of branching in the tibia. Figure 8 is an example of determining the starting point and end-point of branching in the femur and tibia.
6. After the starting point and end-point of the branch are obtained, then the vector length (line) is calculated from these points. The lines are formed from 2 connected points so that a line can be drawn from the furthest branch points on the femoral or tibial area as shown in Figure 9.
7. The length of the vector obtained is used to get an FTA. FTA (θ) is calculated using the following formula:

$$angle\ \theta = arccosine\left(\frac{\overrightarrow{u} . \overrightarrow{v}}{\|u\| . \|v\|}\right) \tag{12}$$

where $\overrightarrow{u} . \overrightarrow{v} = u_1.v_1 + u_2.v_2$; while $\|u\| = \sqrt{u_1^2 + u_2^2}$ and $\|v\| = \sqrt{v_1^2 + v_2^2}$

$\overrightarrow{u}$ is the femoral line, $\overrightarrow{v}$ is the tibial line; while $\|u\|$ is the length of $\overrightarrow{u}$, $\|v\|$ is the length of $\overrightarrow{v}$ and θ is the angle calculated.

Furthermore, the iterative calculation is performed for the angle formed by the intersection of the right femoral line and the right tibial line. Figure 10 shows an example of the iteration required to calculate the FTA using the intersection of the femoral line and the tibial line.

Since the length of the vector is always positive, $\cos \theta$ must have the same sign as the dot product. Thus, if the multiplication of the dot is positive, then $\cos \theta$ is positive, with $\theta < \pi/2$ or 90°. Thus, the corresponding angle is acute. However, if the dot product is negative, then $\cos \theta$ is negative, with $\pi/2 < \theta \leq \pi$ or 90° $< \theta \leq$ 180°. Thus, the corresponding angle is obtuse. After calculating the FTA the condition of the knee is determined according to [14] as follows: varus knee is defined by FTA $\leq$ -2°; a neutral knee by - 2° $<$ FTA $<$ 2° and a valgus knee by FTA $\geq$ 2°.

2.5. Statistical analysis

To find out the adequacy of the data used in this study, we performed a statistical analysis using the Power Analysis method [36]. Additionally, we used statistical analysis to assess the results of our FTA measurement methods, using the FTA from the OAI database. The statistical method used is linear regression and the Bland-Altman plot [17].
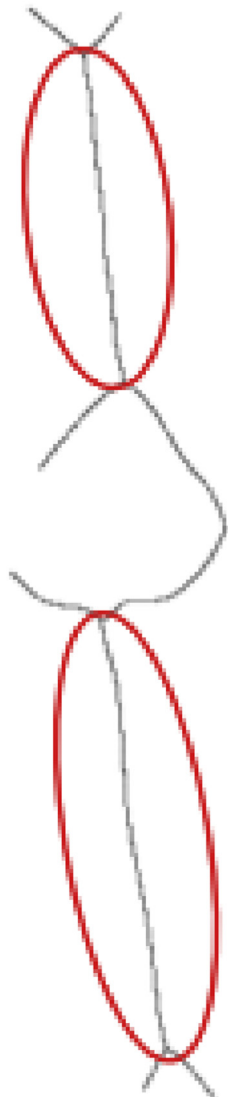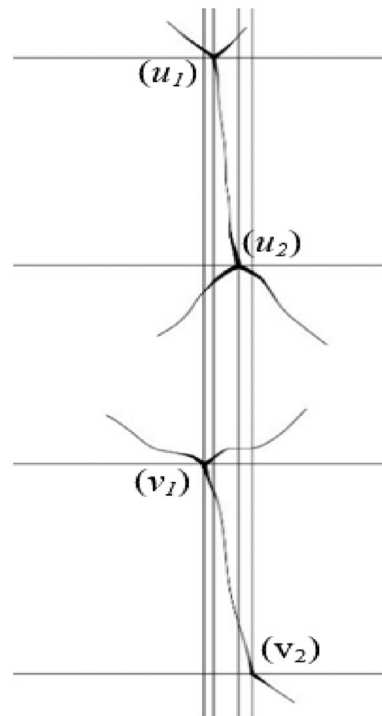

Figure 8. An example of a thinning image to determine the starting point and end-point of branching in the femoral and tibial.

3. Results

In this study, we used 10 training images and 50 testing images from the OAI database. To determine the number of samples used for testing our method, we applied power analysis with Minitab 18. Based on this method using sample Z with known standard deviations from the results
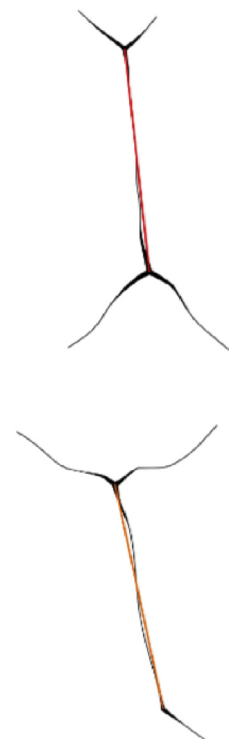

Figure 7. An example of a thinning image that is marked indicates not a branch.

Figure 9. An example of a thinning image to determine vector length both in the femoral and tibial.

of our method FTA, with the FTA obtained from the OAI database, power value 80%, and significance level 5 %, only 30 sample sizes are needed. Additionally, to consider the large number of samples used in this study and to check the results of the experiments can be reproduced, we have randomly selected six test images from 50 test image samples where the results are very good, namely the average difference in the results of FTAs in the first experiment and the second was 0.13° for the right knee and 0.19° for the left knee. Therefore, the number of samples we used is more than enough.

Meanwhile, Table 1 contains the specialty variability of the distance between the ASM and ground truth for measurement of segmentation validation using HD and the overlapping value between ASM segmentation and ground truth using DSC. Based on the experimental results, the average validation of segmentation and the standard deviation using HD were 1.11 mm and 0.15 for the left femoral-tibial, 0.95 mm and 0.07 for the right femoral-tibial while the validation of segmentation and the standard deviation using DSC were 0.91 and 0.02 for left femoral-tibial, 0.95 and 0.01 for right femoral-tibial, respectively.

Table 1 shows that the validation results between ASM segmentation and ground truth using HD obtained 0.84 mm as the best results for the left femoral-tibial on the 20th test image, meanwhile, and the worst result was 1.45 mm on the 19th test image. The best results for the right femoral-tibial were 0.83 mm in the 7th test image, and the worst result was 1.19 mm in the 19th test image. Meanwhile, the results of segmentation validation using DSC obtained 0.95 as the best result for the left femoral-tibial on the 44th test image, and the worst result was 0.87 on the 15th test image. As for the right femoral-tibial, the best result was 0.97 in the 40th test image, and the worst result was 0.92 on the 13th test image.

Furthermore, Figures 11 and 12 are graphs of linear regression modeling on the right and left FTA. Figure 11 shows the trend line with the following equation $y = 0.998 x - 0.051$, which has a minimum average error of 1.543E-14 for the right knee. Meanwhile, Figure 12 shows the trend line with the following equation $y = 0.999 x + 0.014$, which has an average error of 5.085E-16 for the left knee. Figures 11 and 12 show that the points (FTA) produced are close to a straight line. This means that the FTA has followed a normal distribution. In addition, the maximum difference between the FTA value of our algorithm and the OAI database is very small: 0.81° for the right FTA and 0.77° for left FTA. Moreover, in Figure 11, it can also be seen that 82% is a varus knee, 2% a
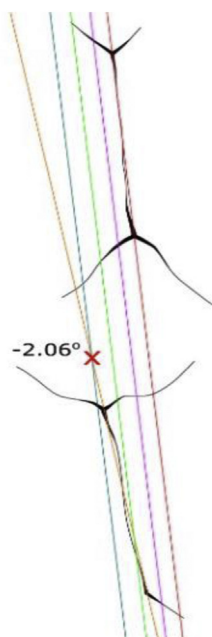
Table 1. Validation of segmentation results using HD and DSC.

No	Name of Image OAI	left femur tibia		right femur tibia	
		HD (mm)	DSC	HD (mm)	DSC
1	9012867	0.92	0.89	0.90	0.95
2	9023193	1.09	0.94	0.95	0.93
3	9034451	0.97	0.91	0.92	0.92
4	9052335	0.95	0.93	0.94	0.94
5	9055836	1.31	0.91	1.12	0.97
6	9070207	1.15	0.88	1.06	0.93
7	9204055	1.23	0.90	0.83	0.95
8	9223590	1.25	0.89	1.06	0.93
9	9235666	1.05	0.89	0.95	0.95
10	9005413	1.14	0.90	0.94	0.95
11	9271965	1.13	0.90	0.93	0.97
12	9291078	1.13	0.90	0.89	0.96
13	9300338	1.22	0.89	0.93	0.92
14	9314101	1.15	0.91	1.06	0.92
15	9015363	1.26	0.87	0.96	0.94
16	9029791	1.26	0.90	0.86	0.96
17	9034963	1.20	0.91	1.05	0.95
18	9039744	0.86	0.88	0.96	0.97
19	9043894	1.49	0.90	1.19	0.96
20	9044788	0.84	0.90	0.94	0.97
21	9349261	1.20	0.90	0.96	0.96
22	9340139	1.21	0.90	0.93	0.95
23	9000099	1.35	0.89	0.95	0.94
24	9014883	0.94	0.91	0.98	0.97
25	9034812	1.31	0.90	0.89	0.95
26	9056326	0.94	0.92	0.87	0.92
27	9081306	0.87	0.89	0.89	0.96
28	9091337	1.14	0.92	0.94	0.95
29	9122643	0.95	0.95	1.11	0.93
30	9124895	0.96	0.91	0.98	0.95
31	9145384	1.12	0.94	0.92	0.96
32	9192540	0.95	0.91	0.95	0.97
33	9215420	1.18	0.90	0.98	0.95
34	9222596	1.18	0.88	0.99	0.95
35	9225592	1.08	0.89	0.88	0.93
36	9248131	1.23	0.90	0.93	0.95
37	9146462	1.22	0.92	0.89	0.95
38	9148828	0.88	0.94	0.99	0.94
39	9215922	1.14	0.92	0.95	0.96
40	9250129	1.16	0.89	0.96	0.97
41	9258562	1.21	0.88	0.93	0.96
42	9263504	1.14	0.93	0.95	0.94
43	9278228	0.84	0.91	0.87	0.96
44	9282257	1.23	0.95	0.93	0.94
45	9301332	1.00	0.90	0.90	0.96
46	9055361	1.27	0.94	0.93	0.97
47	9000798	1.12	0.91	0.92	0.95
48	9086868	1.21	0.90	0.91	0.93
49	9200014	0.93	0.92	0.95	0.96
50	9035779	0.94	0.94	0.98	0.95
	Mean	1.11	0.91	0.95	0.95
	Standard Deviation	0.15	0.02	0.07	0.01

Figure 10. An example of image thinning in determining an FTA.

valgus knee, and 16% a neutral knee, whereas in Figure 12, 88% is a varus knee, 2% is a valgus knee, and 10% is a neutral knee.

Additionally, we also compared the results of FTA measurements using Bland-Altman plots, as shown in Figures 13 and 14. The figures compare the differences in the results of the FTA measurements from the OAI datasets using the new method that we developed. In Figure 13, the
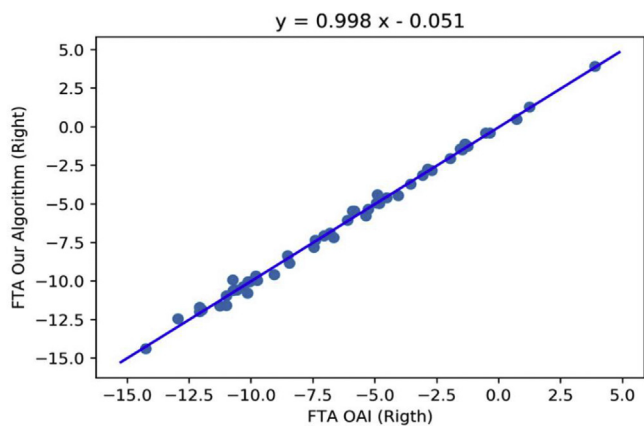
Figure 11. Graph of the FTA in our algorithm and the FTA from the OAI database for the right knee.
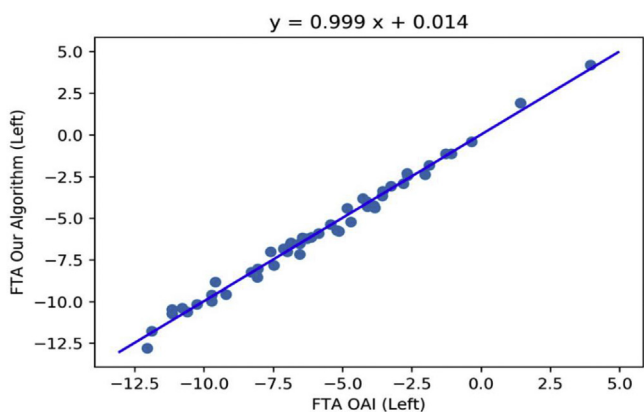

Figure 12. Graph of the FTA in our algorithm and the FTA from the OAI database for the left knee.

mean difference $= -0.04°$; upper Limits of Agreement (LOA) $= 0.52°$; lower LOA $= -0.60°$, and standard deviation $= 0.29°$. The lower LOA difference with mean difference $=$ upper LOA difference with the mean difference, which is $0.56°$. Furthermore, Figure 13 it also shows that there is only one point (FTA measurement results) that is an outlier above the upper LOA and one point below the lower LOA.

Meanwhile, Figure 14 shows the Bland-Altman plot for the left FTA measurement results. In Figure 14, the mean difference $= 0.02°$; upper

LOA $= 0.73°$; lower LOA $= -0.69°$, and standard deviation $= 0.36°$. Lower LOA difference with mean difference $=$ upper LOA difference with the mean difference of $0.71°$. This means that the difference between the two FTA measurement methods is $0.71°$. Additionally, in Figure 14, there is only one point (FTA measurement results) that is an outlier above the upper LOA and one point below the lower LOA.

4. Discussion

As mentioned previously, research on FTA determination has been done in several stages. The purpose of this research is that the results may be used in cases in which a patient present an abnormal FTA, in which the orthopedic physician may suggest interventions that may improve the posture or habits of the patient for improvement of the symptoms and to prevent deterioration of the disease or condition.

Our experimental results show comparable results to the previous work published by Oka et al [10]. These authors demonstrated a difference of flexion FTA equal to $0.86°$ for 20–30 tested images, whereas we showed an FTA difference of $0.81°$ for the right knee and $0.77°$ for the left knee for 50 tested images. Thus, our proposed method shows more reliability concerning the resulting FTA and the number of test images used.

Meanwhile, Iranpour-Boroujeni et al. [12] also used the OAI dataset; however, they showed a slightly worse result with a difference in FTA measurement of $>1°$ between 2 readers. An FTA measurement with fast processing and a small error can provide a clinically relevant tool to assist orthopedic physicians in predicting the risk of occurrence and progression of KOA in patients. Although the current implementation, with 25 s per knee image, is slower than the method previously reported by Iranpour-Boroujeni et al. [12] with 20 s per knee image, we obtained more accurate FTA measurements. Additionally, in our attempt to validate the system developed, namely the stage of femur-tibia segmentation using HD and DSC measurements between semiautomatic segmentation (ASM) and manual segmentation by radiologists as ground truth, the results obtained were outstanding since the difference between the 2 segmentation methods averaged 1 mm of HD and the average using a DSC was 0.9. This results in which DSC> 0.7, are included in the excellent category, as reported by Bharatha et al. [29].

However, the limitation of this study is that there is still one step in the process that is conducted manually, namely segmentation. This step is needed when placing the mean shape as a result of the average training image on each testing image, which is in the center of the cartilage (the connection between the femur and tibia). However, providing clear instructions can minimize the differences in the results of segmentation and FTA between expert segmenters. We required approximately 2–3 s to perform this step. There are many ways in which inter-/intraclass
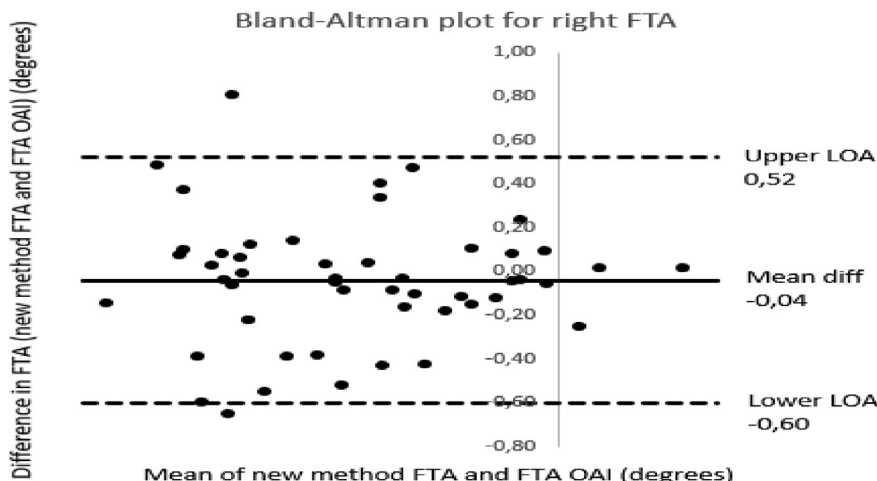

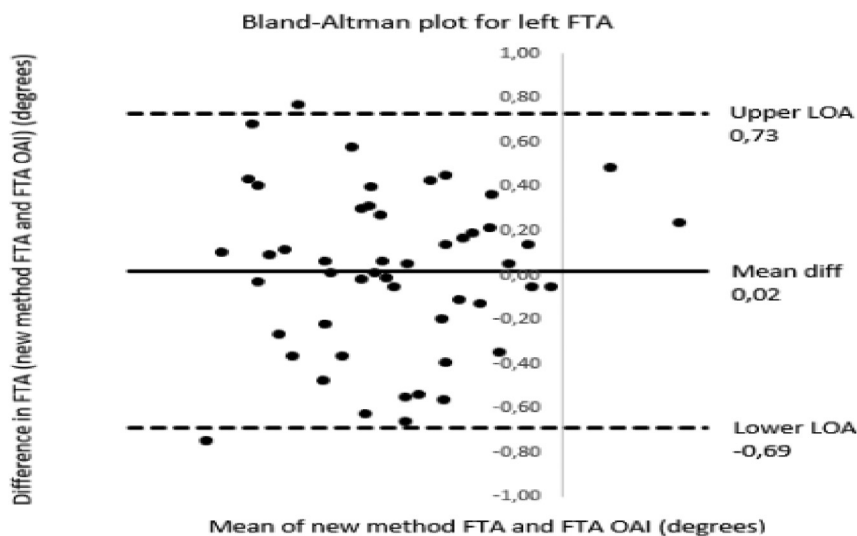**Figure 13.** Bland-Altman plot for the right FTA measurement results.

Figure 14. Bland-Altman plot for the left FTA measurement results.

differences can result during this step of the process. However, we conveyed the rules or instructions for doing this manual step in an attempt to reduce the probability of differences that can occur between expert segmenters. Future work could potentially remove this final manual step.

Another limitation of this method of FTA determination is the low sample rate of 10 training images and 50 testing images. Nevertheless, this sample size was calculated by power analysis and the results show that the number of samples used in this study is more than sufficient. In future studies, more extensive training and testing are required to obtain a more robust clinical tool.

5. Conclusion

The FTA measurements using our algorithm show excellent system performance. The difference in the FTA results compared to the OAI database is very small, namely, below 0.81° for right knee and below 0.77° for left knee, with very minimal average errors. Moreover, the time required to process one image at 25 s is acceptable for use in clinical practice. Accordingly, this method is clinically suitable to measure FTA semi-automatically with only minimal user intervention.

Declarations

Author contribution statement

Rima Tri Wahyuningrum, I Ketut Eddy Purnama: Conceived and designed the experiments; Performed the experiments; Analyzed and interpreted the data; Contributed reagents, materials, analysis tools or data; Wrote the paper.

Gijsbertus Jacob Verkerke: Analyzed and interpreted the data; Wrote the paper.

Peter M.A. van Ooijen, Mauridhi Hery Purnomo: Performed the experiments; Analyzed and interpreted the data; Wrote the paper.

Competing interest statement

The authors declare no conflict of interest.

Additional information

No additional information is available for this paper.

References

[1] WHO | Chronic rheumatic conditions. https://www.who.int/chp/topics/rheumat ic/en/.

[2] D. Hayashi, F.W. Roemer, A. Guermazi, Imaging for osteoarthritis, Ann. Phys. Rehabil. Med. 59 (2016) 161–169.

[3] Z. Xu, J. Bartrina-Rapesta, I. Blanes, V. Sanchez, J. Serra-Sagristà, M. García-Bach, et al., Diagnostically lossless coding of X-ray angiography images based on background suppression, Comput. Electr. Eng. 53 (2016) 319–332.

[4] L. Shamir, S.M. Ling, W.W. Scott, A. Bos, N. Orlov, T.J. Macura, et al., Knee X-ray image analysis method for automated detection of osteoarthritis, IEEE Trans. Biomed. Eng. 56 (2009) 407–415.

[5] J.H. Kellgren, J.S. Lawrence, Radiological assessment of osteo-arthrosis, Ann. Rheum. Dis. 16 (4) (1957) 494–502.

[6] L. Anifah, I.K.E. Purnama, M. Hariadi, M.H. Purnomo, Osteoarthritis classification using self organizing map based on gabor kernel and contrast-limited adaptive histogram equalization, Open Biomed. Eng. J. 7 (2013) 18–28.

[7] R.T. Wahyuningrum, L. Anifah, I.K.E. Purnama, M.H. Purnomo, A novel hybrid of S2DPCA and SVM for knee osteoarthritis classification, in: Comput. Intell. Virtual Environ. Meas. Syst. Appl. (CIVEMSA), 2016 IEEE Int. Conf., IEEE, 2016, pp. 1–5.

[8] R. Riad, R. Jennane, A. Brahim, T. Janvier, H. Toumi, E. Lespessailles, Texture analysis using complex wavelet decomposition for knee osteoarthritis detection: data from the osteoarthritis initiative, Comput. Electr. Eng. 68 (2018) 181–191.

[9] P. Podsiadlo, F.M. Cicuttini, M. Wolski, G.W. Stachowiak, A.E. Wluka, Trabecular bone texture detected by plain radiography is associated with an increased risk of knee replacement in patients with osteoarthritis: a 6 year prospective follow up study, Osteoarthritis Cartilage 22 (1) (2014) 71–75.

[10] T. Janvier, R. Jennane, A. Valery, K. Harrar, M. Delplanque, C. Lelong, D. Loeuille, H. Toumi, E. Lespessailles, Subchondral tibial bone texture analysis predicts knee osteoarthritis progression: data from the osteoarthritis initiative, Osteoarthritis Cartilage 25 (2) (2017) 259–266.

[11] T. Janvier, R. Jennane, H. Toumi, E. Lespessailles, Subchondral tibial bone texture predicts the incidence of radiographic knee osteoarthritis: data from the osteoarthritis initiative, Osteoarthritis Cartilage 25 (12) (2017) 2047–2054.

[12] T. Takahashi, N. Yamanaka, M. Komatsu, Y. Ogawa, S. Yoshida, H. Yamamoto, A new computer-assisted method for measuring the tibio-femoral angle in patients with osteoarthritis of the knee, Osteoarthritis Cartilage 12 (2004) 256–259.

[13] H. Oka, S. Muraki, T. Akune, A. Mabuchi, T. Suzuki, H. Yoshida, et al., Fully automatic quantification of knee osteoarthritis severity on plain radiographs, Osteoarthritis Cartilage 16 (2008) 1300–1306.

[14] A.K.O. Wong, D. Inglis, K.A. Beattie, A. Doan, G. Ioannidis, J. Obeid, et al., Reproducibility of computer-assisted joint alignment measurement in OA knee radiographs, Osteoarthritis Cartilage 17 (2009) 579–585.

[15] G. McDaniel, K.L. Mitchell, C. Charles, V.B. Kraus, A comparison of five approaches to measurement of anatomic knee alignment from radiographs, Osteoarthritis Cartilage 18 (2010) 273–277.

[16] L. Sheehy, D. Felson, Y. Zhang, J. Niu, Y.-M. Lam, N. Segal, et al., Does measurement of the anatomic axis consistently predict hip-knee-ankle angle (HKA) for knee alignment studies in osteoarthritis? Analysis of long limb radiographs from the multicenter osteoarthritis (MOST) study, Osteoarthritis Cartilage 19 (2011) 58–64.

[17] T. Iranpour-Boroujeni, J. Li, J.A. Lynch, M. Nevitt, J. Duryea, A new method to measure anatomic knee alignment for large studies of OA: data from the Osteoarthritis Initiative, Osteoarthritis Cartilage 22 (2014) 1668–1674.

[18] L.M. Goulston, M.T. Sanchez-Santos, S. D'Angelo, K.M. Leyland, D.J. Hart, T.D. Spector, et al., A comparison of radiographic anatomic axis knee alignment measurements and cross-sectional associations with knee osteoarthritis, Osteoarthritis Cartilage 24 (2016) 612–622.

[19] G.M. Brouwer, A.W. Van Tol, A.P. Bergink, J.N. Belo, R.M.D. Bernsen, M. Reijman, et al., Association between valgus and varus alignment and the development and progression of radiographic osteoarthritis of the knee, Arthritis Rheum. 56 (2007) 1204–1211.

[20] B. Xu, Y. Zhuang, H. Tang, L. Zhang, Object-based multilevel contrast stretching method for image enhancement, IEEE Trans. Consum. Electron. 56 (2010).

[21] D. Kim, C. Kim, Contrast enhancement using combined 1-D and 2-D histogram-based techniques, IEEE Signal Process. Lett. 24 (2017) 804–808.

[22] J.A. Lynch, N. Parimi, R.K. Chaganti, M.C. Nevitt, N.E. Lane, The association of proximal femoral shape and incident radiographic hip OA in elderly women, Osteoarthritis Cartilage 17 (2009) 1313–1318.

[23] B.L. Wise, F. Liu, L. Kritikos, J.A. Lynch, N. Parimi, Y. Zhang, et al., The association of distal femur and proximal tibia shape with sex: the Osteoarthritis Initiative, Semin. Arthritis Rheum. 46 (2016) 20–26.

[24] B.L. Wise, L. Kritikos, J.A. Lynch, F. Liu, N. Parimi, K.L. Tileston, et al., Proximal femur shape differs between subjects with lateral and medial knee osteoarthritis and controls: the Osteoarthritis Initiative, Osteoarthritis Cartilage 22 (2014) 2067–2073.

[25] Tim Cootes, Er Baldock, An introduction to active shape models, Image Process. Anal. (2000) 223–248.

[26] B. van Ginneken, A.F. Frangi, J.J. Staal, B.M. ter Haar Romeny, M.A. Viergever, Active shape model segmentation with optimal features, IEEE Trans. Med. Imag. 21 (2002) 924–933.

[27] S.S. Soh, T.T. Swee, S.S. Ying, C.Z. En, M.N. bin Mazenan, L.K. Meng, Magnetic resonance image segmentation for knee osteoarthritis using active shape models, in: Biomed. Eng. Int. Conf. (BMEiCON), 2014 7th, IEEE, 2014, pp. 1–5.

[28] M. Seise, S.J. McKenna, I.W. Ricketts, C.A. Wigderowitz, Learning active shape models for bifurcating contours, IEEE Trans. Med. Imag. 26 (2007) 666–677.

[29] B. Maan, F. van der Heijden, Prostate MR image segmentation using 3D active appearance models. in PROMISE 12 : Miccai 2012 Grand Challenge on Prostate MR Image Segmentation. Grand Challenges in Medical Image Analysis, PROMISE12, 2012, pp. 44–51.

[30] A.A. Taha, A. Hanbury, An efficient algorithm for calculating the exact Hausdorff distance, IEEE Trans. Pattern Anal. Mach. Intell. 37 (2015) 2153–2163.

[31] A. Bharatha, M. Hirose, N. Hata, S.K. Warfield, M. Ferrant, K.H. Zou, E. Suarez-Santana, J. Ruiz-Alzola, A. D'Amico, R.A. Cormack, R. Kikinis, F.A. Jolesz, C.M. Tempany, Evaluation of three-dimensional finite element-based deformable registration of pre- and intraoperative prostate imaging, Med. Phys. 28 (12) (2001) 2551–2560.

[32] K.H. Zou, S.K. Warfield, A. Bharatha, C.M.C. Tempany, M.R. Kaus, S.J. Haker, W.M. Wells III, F.A. Jolesz, R. Kikinis, Statistical validation of image segmentation quality based on a spatial overlap index, Acad. Radiol. 11 (2) (2004) 178–189.

[33] X. Zhenzhen, B. Tao, Y. Li, J. Zhang, X. Qu, F. Cao, J. Liang, 3D fusion framework for infarction and angiogenesis analysis in a myocardial infarct minipig model, Mol. Imag. 16 (2017) 1–10.

[34] C. Wen, G. Ao, Y. Tian, A thinning method for fingerprint image based on Hit-Miss Transformation, in: Comput. Sci. Autom. Eng. (CSAE), 2011 IEEE Int. Conf., Vol. 1, IEEE, 2011, pp. 225–228.

[35] P. Murray, S. Marshall, Chapter five: a review of advances in the hit-or miss transform, Adv. Imag. Electron. Phys. 175 (2013) 221–282.

[36] E. Bagiella, H. Chang, Power analysis and sample size calculation, J. Mol. Cell. Cardiol. 133 (2019) 214–216.